

# Phosphatidylserine as a tumor target for CAR-T cell therapy

Celia Martín-Otal,<sup>1</sup> Inés Sánchez-Moreno,<sup>1</sup> Alvaro Gómez-Morón ,<sup>2</sup> Carla Castro,<sup>1</sup> Noelia Casares,<sup>1</sup> Flor Navarro,<sup>1</sup> Marta Gorraiz,<sup>1</sup> Pedro Justicia-Lirio,<sup>1</sup> Felix Pareja,<sup>3</sup> María Collantes,<sup>3</sup> Iván Peñuelas,<sup>3</sup> Mercedes Iñarrairaegui,<sup>4,5</sup> Bruno Sangro,<sup>4,5</sup> Isabel Vivas,<sup>4,6</sup> Marta Larrayoz ,<sup>4,7</sup> Juan Roberto Rodriguez,<sup>4,7</sup> Felipe Prosper,<sup>4,8</sup> Sandra Hervas-Stubbs ,<sup>1,4</sup> Noa Martín-Cofreces,<sup>9</sup> Juan Jose Lasarte ,<sup>1,4</sup> Teresa Lozano<sup>1,4</sup>

**To cite:** Martín-Otal C, Sánchez-Moreno I, Gómez-Morón A, *et al.* Phosphatidylserine as a tumor target for CAR-T cell therapy. *Journal for ImmunoTherapy of Cancer* 2025;**13**:e009468. doi:10.1136/jitc-2024-009468

► Additional supplemental material is published online only. To view, please visit the journal online (<https://doi.org/10.1136/jitc-2024-009468>).

Accepted 03 February 2025

## ABSTRACT

**Background** Phosphatidylserine (PS) exposed on apoptotic cells promotes immune clearance of dead cells without inducing inflammation. Conversely, PS exposure on live tumor cells promotes an immunosuppressive tumor microenvironment that hinders antitumor immune responses. After confirming elevated PS levels in various tumor cell lines and cancer tissues, we aimed to investigate its potential as a target antigen for chimeric antigen receptor T cell (CAR-T) therapy.

**Methods** We used two different approaches to target PS. First, we employed the adaptor proteins, EDAnnexin or BCMAnnexin comprising annexin V and EDA (extra domain A of fibronectin) or B-cell maturation antigen (BCMA) antigens, to redirect the lytic activity of EDA CAR-T or BCMA CAR-T cells toward PS-expressing tumor cells. In a second approach, we developed an annexin V-based CAR (Anxa CAR-T) to directly recognize PS-positive tumor cells.

**Results** The adaptor proteins EDAnnexin and BCMAnnexin successfully redirected EDA CAR-T or BCMA CAR-T cell activity, leading to an efficient recognition of PS<sup>+</sup> tumor cells in vitro. However, the established immunological synapse differs significantly from that observed when CAR-T cells recognize the tumor cells directly. In vivo administration of the adaptor proteins, combined with the corresponding CAR-T cells, displayed antitumor activity in mice bearing PS<sup>+</sup> tumors. Regarding the second approach, Anxa CAR-T cells effectively recognized and killed PS<sup>+</sup> tumor cells in vitro. Nonetheless, PS exposure on T-cell membranes during T-cell activation impeded efficient Anxa CAR-T cell manufacturing due to fratricide. By optimizing retroviral dose to reduce Anxa CAR expression on the cell membrane, or by using the multikinase inhibitor dasatinib, the fratricide effect was mitigated, enabling successful Anxa CAR<sup>Low</sup>-T cell production. Remarkably, Anxa CAR<sup>Low</sup>-T cells demonstrated antitumor activity in in vivo murine models of PS<sup>+</sup> hepatocarcinoma and teratocarcinoma. No signs of toxicity were observed after Anxa CAR-T cell administration.

**Conclusions** PS holds promise as a target antigen for CAR-T cell therapy, underscoring the need to address fratricide as a key challenge in the development of PS-targeting CAR-T cells.

## WHAT IS ALREADY KNOWN ON THIS TOPIC

⇒ Externalization of phosphatidylserine (PS) in tumors, due to nutrient deprivation, oxidative stress, and hypoxia can contribute to the induction of an immunosuppressive tumor microenvironment.

## WHAT THIS STUDY ADDS

⇒ We have shown that PS is highly expressed in various tumor cell lines and tumor tissues, especially in cells with a high proliferation rate, making it a promising target for chimeric antigen receptor (CAR-T cell-based therapies). Leveraging the strong affinity of annexin V for PS, we engineered the Anxa CAR-T to effectively recognize PS in tumor cells. Nonetheless, transient and mild exposure of PS in T cells post-stimulation can trigger a fratricide effect during the CAR-T manufacturing process. This fratricide can be mitigated by reducing Anxa CAR expression levels on T-cell membrane or by blocking CAR signaling with the kinase inhibitor dasatinib.

## HOW THIS STUDY MIGHT AFFECT RESEARCH, PRACTICE OR POLICY

⇒ Anxa CAR-T cells show promise in targeting a high variety of proliferating tumor cells by recognizing PS exposed on their surface. This suggests a potential use for the treatment of a broad range of cancer types.

## INTRODUCTION

One of the main challenges for the translation of chimeric antigen receptor (CAR)-T cell-based therapies to the treatment of solid tumors is the identification of specific antigens expressed on the tumor cell membrane. In this work, we focused on phosphatidylserine (PS), an essential component in all human cells that, although it is normally present on the inner face of the cell membrane, it can be exposed in the outer face of tumor cells in response to a variety of external and internal stimuli. PS externalization is a marker of early cell apoptosis and serves as an “eat-me signal”



© Author(s) (or their employer(s)) 2025. Re-use permitted under CC BY-NC. No commercial re-use. See rights and permissions. Published by BMJ Group.

For numbered affiliations see end of article.

## Correspondence to

Dr Juan Jose Lasarte; [jjlasarte@unav.es](mailto:jjlasarte@unav.es)



for efferocytosis by macrophages allowing controlled and silent removal of damaged or senescent cells.<sup>1</sup> PS is recognized directly by the T-cell/transmembrane immunoglobulin and mucin (TIM) family of receptors or indirectly by TAM receptors (rTAM: type I receptor-tyrosine kinases Tyro3, AXL or MerTK) using Gas6 and protein S (ProS) as “bridge” molecules that bind the receptor to PS.<sup>2,3</sup> Both types of receptors elicit an immunosuppressive effect on immune cells, including MDSCs (Myeloid-derived suppressor cells), CD4<sup>+</sup> and CD8<sup>+</sup> T cells, DCs (Dendritic cells), macrophages, B cells, and natural killer (NK) cells.<sup>4,5</sup> Thus, the externalization of PS in apoptotic cells promotes the elimination of apoptotic bodies, maintaining tissue homeostasis without causing pathological inflammation. However, PS externalization in tumors is highly deregulated by the combined action of nutrient deprivation, oxidative stress, and hypoxia,<sup>6–8</sup> having an undesired immunosuppressive effect. Therefore, therapeutic disruption of PS/rTAMs interactions may represent a potential strategy to inhibit tumor progression.<sup>6</sup>

Annexin A5 (annexin V) is a member of the calcium-dependent annexin family of phospholipid-binding proteins. It has a strong affinity for PS, making it a useful marker for identifying apoptotic cells. Furthermore, annexin V binding to apoptotic PS<sup>+</sup> cells can reduce the immunosuppressive effects mediated by PS, enhance the immunogenicity of apoptotic cells,<sup>9</sup> and improve the efficacy of tumor antigen-specific immunotherapies, especially following cytotoxic chemotherapy that increases the exposure of PS on tumor cells.<sup>10</sup>

In this work, we used annexin V to design CAR-T cell-based therapies to target PS<sup>+</sup> tumor cells. Initially, we employed an adaptor-CAR-T system approach to redirect the cytotoxic activity of CAR-T cells. This method uses a bi-functional fusion protein comprising annexin V to target PS in tumors and a specific antigen recognized by a previously validated CAR-T cell.<sup>11</sup> As a second approach, we designed a chimeric receptor based on the use of annexin V as the CAR ectodomain and the CD3 $\zeta$  and CD137 endodomains (Anxa CAR-T). We found that activated CAR-T cells also externalize significant levels of PS triggering a fratricide effect during the Anxa CAR-T cell manufacturing process. We have seen that Anxa CAR-T cells can be more efficiently produced by reducing the level of Anxa CAR expression in the T-cell membrane or by inhibiting the CAR signaling using tyrosine kinase inhibitors. These Anxa CAR<sup>low</sup>-T cells exerted antitumor activity in vivo in murine tumor models of hepatocarcinoma or teratocarcinoma.

## MATERIALS AND METHODS

### Mice

Female C57BL/6J mice were purchased from Harlan Laboratories. 129Sv mice were obtained from Janvier Laboratory (Le Genest Saint Isle, France). Animal handling and tumor experiments were carried out in accordance with our institutional ethics committee's

guidelines (Ref: 019–19) and in compliance with the European Directive 2010/63/EU.

### Cell lines

The murine HCC PM299L (provided by Dr Lujambio, New York, USA), the melanoma B16F10 (American Type Culture Collection, ATCC), the murine multiple myeloma MM5080 and MM8273 (Dr José A Martínez-Clement, Pamplona, Spain), the Lewis lung carcinoma cells (Dr Ajona, Pamplona, Spain), the teratocarcinoma cell line F9 (ATCC) and the pancreatic ductal adenocarcinoma cell line FC1242 (Dr S Vicent, Pamplona, Spain) were cultured in complete medium (RPMI 1640 (Roswell Park Memorial Institute 1640) or DMEM (Dulbecco's Modified Eagle Medium) containing 10% FBS (Fetal bovine serum), antibiotics, 2 mM glutamine and 50  $\mu$ M 2-ME). The Platinum Ecotropic (Plat-E, ATCC) cell line was cultured in DMEM supplemented with 10% FBS and the selection antibiotics puromycin (100  $\mu$ g/mL) and blasticidin (10  $\mu$ g/mL). All cell lines were cultured at 37°C in a humidified atmosphere with 6.5% CO<sub>2</sub>. In some experiments, cell lines were incubated for 4 hours at 37°C in SILAC medium (lysine and arginine deficient media supplemented with lyophilized serum) or incubated at 37°C after 60 Gy irradiation to evaluate the impact on PS expression.

### Plasmids and retroviral transduction

Anxa CAR construct is composed of the annexin V protein sequence as a CAR recognition site followed by a murine 4-1BB-CD3 $\zeta$  expression cassette linked through an F2A self-cleaving peptide sequence to eGFP (enhanced green fluorescence protein). The extra domain A of fibronectin (EDA) CAR containing the anti-EDA F8 single-chain variable fragment of an antibody (scFv) was described in a previous work.<sup>11</sup> The PSMA CAR (specific for Prostate-Specific Membrane Antigen), used as an irrelevant CAR, included the anti-human PSMA scFv (from mouse hybridoma J591), that was cloned in the same expression cassette.

For retrovirus productions, Plat-E cells were transfected with 5  $\mu$ g of retroviral plasmid DNA along with 2.5  $\mu$ g pCLEco plasmid DNA using Lipofectamine 2000 (Invitrogen) for 6 hours in antibiotic-free medium as previously described.<sup>12</sup> Retroviral supernatants were collected at 48 and 72 hours after transfection.

### Murine CAR-T cells generation

Purified murine CD4<sup>+</sup> and CD8<sup>+</sup> T cells were activated with dynabeads CD3/CD28 at a 1:2 (bead:T cell) cell ratio for 24 hours in RPMI complete media containing 100 IU/mL recombinant human interleukin-2 (rhIL-2). 24 hours later, T cells were retrovirally infected, incubated with 100 IU/mL rhIL-2 and 10  $\mu$ g/mL protamine sulfate (Sigma) and spun at 1,300 $\times$ g at 32°C for 90 min as described previously.<sup>11</sup> Infection was repeated 1 day later. After infection, lymphocytes were cultured in a complete RPMI medium with rhIL-2 until day 5 and used

for functional *in vitro* or *in vivo* assays. Transduction efficiency was assessed by reporter gene expression using flow cytometry (FACS).

### Antibodies and flow cytometry

Samples were analyzed using an FACSCanto II flow cytometer (Becton Dickinson) and data were evaluated with FlowJo software (Tree Star). Anti-annexin V antibody (EPR3980) (Abcam) and goat anti-rabbit IgG secondary antibody (BioLegend) were used to detect Anxa CAR by flow cytometry. For cell viability, cells were incubated with the Zombie-NIR Fixable Viability Kit (BioLegend) for 15 min at room temperature (RT) and then washed once with washing buffer. For PS detection, cells were incubated with APC (Allophycocyanin) annexin V (BD Biosciences) in annexin-binding buffer containing  $\text{Ca}^{2+}$  for 15 min at RT.

T-cell phenotype was assessed by using the following fluorochrome-conjugated antibodies (BioLegend) at 0.25–1  $\mu\text{g}/\text{mL}$ : CD8a (53–6.7), CD4, (RM4-5), CD69 (H1.2F3), CD44 (IM7), CD62L (MEL-14), CD137 (17B5), PD-1 (29F.1A12), TIM3 (B8.2C12) and LAG3 (C9B7W) (online supplemental table 1). For staining, cells were incubated with the Zombie NIR Fixable Viability Kit (BioLegend) for 15 min at RT and then washed once with washing buffer. Cells were fixed and permeabilized buffer (BD) and then stained intracellularly (15 min, RT) with fluorochrome-conjugated monoclonal antibodies (mAbs) against mouse Tumor Necrosis Factor- $\alpha$  (TNF- $\alpha$ ) (MP6-XT22) and IFN- $\gamma$  (XMG1.2).

### Expression and purification of recombinant proteins

DNA sequences coding for annexin V, for the EDA-annexin V (EDAnnexin), or for BCMA-annexin V (BCMAnnexin) fusion proteins were cloned in pET20b plasmid (Novagen), which enables expression of proteins carrying six histidine residues at the carboxyl terminus. The resulting plasmids were transfected into BL21(DE3) transformed by a heat shock according to manufacturer's instructions (Novagen) cells, for the expression of the recombinant proteins which were purified by affinity chromatography (HisTrap columns, Amersham Biosciences) according to the manufacturer's instructions using a fast protein liquid chromatography platform (AKTA; Pharmacia). Purified proteins were analyzed by Coomassie and western blot using anti-His antibodies. Recognition of EDAnnexin or BCMAnnexin by the purified scFv F8 (specific for EDA protein<sup>13</sup>) was tested by ELISA using plates coated with different concentrations of the proteins as described previously.<sup>11</sup> In addition, binding of EDAnnexin and BCMAnnexin to  $\text{PS}^+$  tumor cells (by annexin V fragment), to EDA CAR-T cells (by EDA fragment) or to B-cell maturation antigen (BCMA) CAR-T cells (by BCMA) was analyzed by flow cytometry with anti-His-APC antibody after incubation with the recombinant protein as previously described.<sup>14</sup>

### Protein radiolabeling

70  $\mu\text{g}$  (100  $\mu\text{L}$ ) of EDA-OVA were radiolabeled with 17.4 MBq of  $(^{99\text{m}}\text{Tc}(\text{CO})_3(\text{H}_2\text{O})_3)^+$ , previously prepared by adding freshly eluted  $(^{99\text{m}}\text{Tc})\text{TcO}_4\text{Na}$  into a tricarbonyl kit (CRS, Paul Scherer Institut PSI, Villigen, Switzerland) which was incubated at 100°C (30 min) and later at 25°C for 15 min. EDAnnexin (140  $\mu\text{g}$  in 200  $\mu\text{L}$ ) were radiolabeled with 14 MBq of  $(^{99\text{m}}\text{Tc})\text{NaTcO}_4$ , using 40  $\mu\text{L}$  of 5 mg/mL  $\text{SnCl}_2$  as a reducing agent. Radiochemical purity was checked by RadioTLC (ITLC-SG, Sodium Citrate 0.1 M) and it was >96% in both cases. No further purification was required.

### Single photon emission CT/CT *in vivo* biodistribution studies

For protein biodistribution studies, each animal received one single dose of the radiolabeled protein by intravenous injection (EDAnnexin: 3.7 MBq; n=2; EDA-OVA: 11 MBq, n=1). After this, single photon emission CT (SPECT) scans were acquired in a U-SPECT6/E-class (MILabs) 1, 3, 6 and 22 hours post-administration using an ultrahigh resolution collimator. For image acquisition, animals were placed prone on the scanner bed under continuous anesthesia with isoflurane (2% in 100%  $\text{O}_2$  gas) and a scan in list mode format was acquired over 30 min covering a portion of the body from the liver to the middle portion of the hind limbs. Following the SPECT acquisition, CT scans were performed to obtain anatomical information using a tube setting of 55 kV and 0.33 mA. SPECT images were reconstructed using the technetium-99m photopeak with a 20% energy window width and using a calibration factor to obtain the activity information (MBq/mL); then, the attenuation correction was performed using the CT attenuation map. Studies were visualized using PMOD software as described previously<sup>15</sup> (PMOD Technologies, Adliswil, Switzerland).

To properly compare the different sets of images, the technetium-99m decay was corrected using a numerical factor, and then images were transformed to SUV units (SUV: standardized uptake value), using the formula  $\text{SUV} = (\text{tissue activity concentration (MBq}/\text{cm}^3) / \text{injected dose (MBq)}) \times \text{bodyweight (g)}$ .

### Characterization of CAR-T cells

The *in vitro* functional characterization of CAR-T cells, including their ability to express the CAR on the cell surface, recognize EDAnnexin and  $\text{PS}^+$  tumor cells coated with EDAnnexin and proliferate, produce IFN- $\gamma$  or IL-2, or kill tumor cells was carried out as previously described<sup>11 16 17</sup> and in online supplemental methods. *In vivo* assessment of antitumor activity of EDA CAR-T cells by EDAnnexin fusion protein or directly by Anxa CAR-T cells was carried out in mice bearing F9 teratocarcinoma or PM299L hepatocarcinoma tumors as described in online supplemental methods.

### Live cell imaging

$\text{CD4}^+$  and  $\text{CD8}^+$  CAR-T expressing high or low levels of the CAR construct as well as untransduced T cells were

labeled with LysoTracker Red DND-99 probe (1  $\mu$ M, Thermo Fisher Scientific) in complete medium (RPMI 1640 10% FBS) for 1 hour at 37°C. Cells were then washed with a complete medium and resuspended in an imaging medium (RPMI 1640 without phenol red, 2% FBS, 25 mM HEPES (4-(2-Hydroxyethyl)-1-piperazineethanesulfonic acid).  $10^5$  cells were plated in glass-bottom 96-well plates (iBidi) pre-coated with 10  $\mu$ g/mL fibronectin from human plasma in RPMI for 18 hours at 4°C. The different cells were plated simultaneously and recording was initiated 5 min after plating. Epifluorescence images were acquired as a Z-series of fluorescence and brightfield images (THUNDER Imager Live Cell) and deconvolved with the accompanying Thunder algorithm (Leica Microsystems). A 63 $\times$  immersion oil objective was used. Images were acquired every 45 s for 1 hour. Data were analyzed with Image J software (<http://rsbweb.nih.gov/ij/>). LysoTracker Red mean fluorescence intensity (MFI) and apoptotic cell ratios at initial and final times were determined for degranulation and fratricide effect.

### Immunofluorescence and analysis of immunological synapse

PM299L cells expressing EDA antigen were plated in glass-bottom-8-well plates (iBidi) pre-coated with 10  $\mu$ g/mL fibronectin. Transduced CAR CD8 T cells were allowed to conjugate with the tumor cells for 10 min and fixed with paraformaldehyde PFA (1%) for 10 min. Then cells were stained with anti-Giantin rabbit antibody (for Golgi staining, Abcam) followed by highly-crossadsorbed anti-rabbit Alexa-568 and Alexa-647-conjugated phalloidin (for F-actin staining, Molecular Probes, Invitrogen) in PHEM as described.<sup>18</sup> Fluorescence and brightfield images were acquired with a Leica SP8 Navigator confocal microscope equipped with a pulsed WLL (range, 470–670 nm) and an HC PL Apo CS2 100 $\times$ /1.4 oil objective, controlled by accompanying Application Suite X software (LAS X, 3.5.2.18963; Leica Microsystems GmbH). Three-dimensional reconstructions of cells, volume rendering and quantification of Golgi-IS distance were performed with IMARIS V.8.4 software (<https://imaris.oxinst.com>). Polarization of F-actin was calculated using the Fiji plugin “Synapse measure” (<http://rsbweb.nih.gov/ij/>).<sup>19</sup>

### Statistical analysis

Normality was assessed with Shapiro-Wilk W test. Statistical analyses were performed using parametric Student's t-test, two-tailed paired t-test, and one-way or two-way analysis of variance with Bonferroni multiple comparison test, as indicated. Mann-Whitney U and Kruskal-Wallis were used for non-parametric analyses. For tumor growth, data were analyzed using non-linear third-order polynomial (cubic) regression curves. A p value of <0.05 was regarded as statistically significant for all tests. Continuous variables were presented as means $\pm$ SD. Statistical analysis was performed using GraphPad Prism V.9 (GraphPad Software).

## RESULTS

### PS is exposed in tumor cell lines and binds annexin V

We first analyzed the exposure of PS in the outer cell membrane of a panel of mouse and human tumor cell lines from different origin including pancreatic cancer (FC12142 and PM12500) hepatocarcinoma (PM299L and PLC), lung carcinoma (LLCOVA), teratocarcinoma (F9), cholangiocarcinoma (TFK1 and HUCCT), melanoma (B16OVA) or multiple myeloma (MM8273 and MM5080 cell lines) using APC-conjugated annexin V staining. Mouse splenocytes or human lymphocytes were also included in the analysis. Expanding the results of previous reports, we found high levels of PS exposure in almost all tumor cell lines tested (figure 1A,B for mouse and human cell lines, respectively). In most cases, both nutrient deprivation (SILAC) as well as irradiation (60 Gy) enhanced annexin V exposure in the outer membrane. We also analyzed the level of annexin V staining ex vivo in splenocytes isolated from C57BL/6 naïve mice as well as in tumor homogenates isolated from mice bearing F9, FC1242, PM299L and LLCOVA tumors before or 24 hours after 4 Gy total body irradiation (TBI). It was found that 20–40% of alive tumor cells (Zombie NIR<sup>-</sup> cells) were annexin V positive, suggesting the expression of PS in the outer side of the tumor cell membrane. Although not statistically significant, TBI had a detectable enhancement in annexin V staining, in particular in F9 and LLCOVA tumors (figure 1C). Interestingly, the percentage of PS<sup>+</sup> cells in healthy tissues such as the bone marrow, liver, lymph nodes, lung, spleen, and thymus ranged from less than 5% (lung) to 12.5% (spleen), with a slight increase observed after TBI (online supplemental figure 1), and clearly lower than those observed in tumor tissues. Importantly, when we compared the MFI of annexin V staining in EpCAM<sup>+</sup>CD45<sup>-</sup>NIR<sup>-</sup> cells between the tumor and non-tumor areas in five human hepatocarcinoma resection samples, we observed a significant increase in annexin V staining within the tumor region (figure 1D).

### PS exposure is associated with a high replication ratio of cells

To investigate the kinetics of PS exposure during cell proliferation, we conducted a titration experiment using the <sup>3</sup>H-thymidine incorporation method and simultaneously assessed PS exposure levels in tumor cell lines. Our findings indicated a direct correlation between the proliferation rate (cpm/cell) of the tumor lines and PS exposure on their membranes (figure 1E). This trend was confirmed by flow cytometry analysis of PS exposure in Ki-67<sup>+</sup> cells (figure 1F). Notably, fewer seeded cells led to higher proliferative indices and greater PS exposure. These results suggest that proliferation stress enhances PS exposure. Additionally, immunohistochemical staining for the proliferation marker Ki-67 in tumor sections from mice bearing tumors derived from these tumor cell lines showed 25–60% Ki-67 positivity (figure 1G,H). It is tempting to speculate that PS exposure in tumor tissue cells is a dynamic process that depends on their

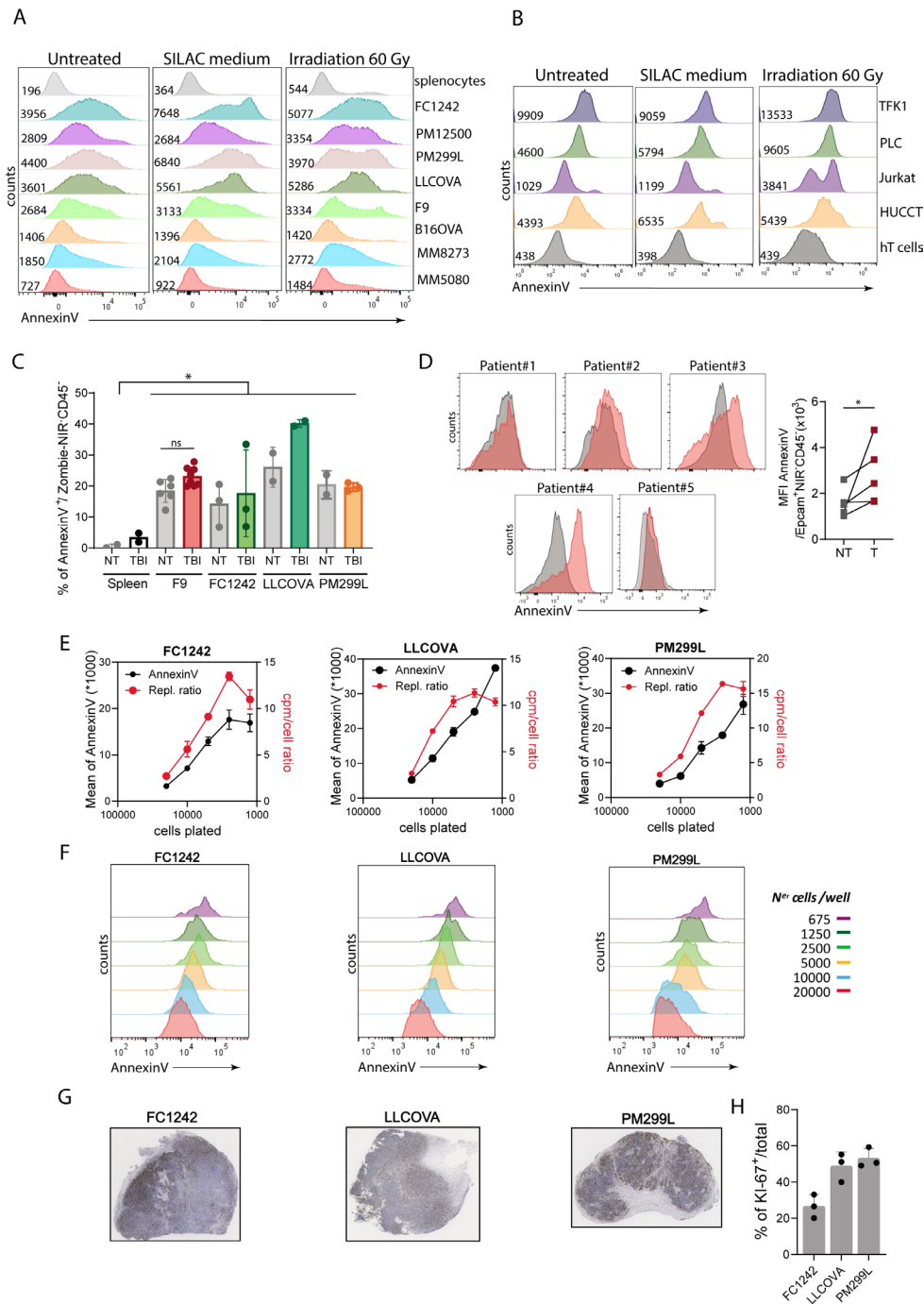


**Figure 1** PS expression in different tumor cell lines and tumor tissues. (A) PS expression in murine (A) and human (B) tumor cell lines was analyzed using flow cytometry with annexin V staining. The analysis included cells incubated in standard culture medium (untreated), nutrient-deprived SILAC medium, or following irradiation. Primary lymphocytes were also included as controls. Numbers indicate the mean fluorescence intensity for each condition. The results are representative of three independent experiments. (C) PS exposure in tumors isolated from mice previously challenged with F9, FC1242, LLCOVA or PM299L tumor cell lines. The effect of total body irradiation with 4 Gy (TBI) 24 hours before tumor extraction was also evaluated. Bars representing the mean and SD are plotted. (D) PS exposure, indicated by the MFI of annexin V staining in EpCAM<sup>+</sup>CD45<sup>-</sup>Zombie-NIR<sup>-</sup> cells, was measured in tumor resections of five patients with hepatocellular carcinoma. Each histogram corresponds to one patient, with annexin V staining in the non-tumor (NT) area shown in gray and the staining corresponding to the tumor area shown in color (T). The graph represents the analysis of paired samples from these five patients. (E) Tumor cell proliferation rate (<sup>3</sup>H-thymidine incorporation (cpm/cell)) and PS exposure levels in the indicated tumor cell lines plated at different cell densities. (F) PS exposure in Ki-67<sup>+</sup> cells. (G) Immunohistochemical staining for Ki-67 in FC1242, LLCOVA or PM299L tumor tissue sections and their quantification (H). Numbers in the histogram are MFI (A, B). Data are representative of two to three independently repeated experiments. One-way analysis of variance and Bonferroni as a post hoc test (C). paired t-test (D). \*p<0.05. MFI, mean fluorescence intensity; NT, non-treated; ns, no significance; PS, phosphatidylserine; TBI, total body irradiation.

proliferative status or the cellular stress they are experiencing at any given moment.

### Annexin V-based adaptor proteins to redirect CAR-T cell activity

After verifying that PS can be considered as a tumor-associated antigen and, based in the capacity of annexin V protein to bind PS with high affinity, we valued the possibility of generating an annexin V-containing adaptor protein to redirect towards PS the activity of a CAR with another specificity. In a previous work, we generated a CAR-T targeting the EDA, which is expressed in the extracellular matrix (ECM) of various tumors but not in healthy tissues.<sup>11</sup> Since EDA is not expressed in the tumor cell membrane, we evaluated the possibility of targeting PS<sup>+</sup> tumor cells with EDA CAR-T cells by using the adaptor protein EDA-annexin V (EDAnnexin) (figure 2A).

EDA, annexin V and EDAnnexin proteins (putative MW of 10, 38 and 48 kD, respectively) were produced and purified from *Escherichia coli* BL21 (DE3) cells (figure 2B). The capacity of the fusion proteins to be recognized by the anti-EDA scFv included in the EDA CAR construct was assessed by ELISA. It was found that both proteins EDA and EDAnnexin were well recognized by the scFv, indicating that the EDA domain was well exposed in the EDAnnexin fusion protein (figure 2C). Next, we evaluated by flow cytometry the ability of EDAnnexin to bind to PS on the surface of the LLCOVA, FC1242 and F9 tumor cell lines. It was verified that EDAnnexin was able to bind to the three tumor cell lines (figure 2D).

Next, EDA CAR-T cells and control PSMA CAR-T cells were prepared to assess their ability to recognize the EDAnnexin protein and induce CAR-T cell activation. Both CD4 and CD8 EDA CAR-T cells, but not PSMA CAR-T cells, exhibited a robust production of IFN- $\gamma$  in response to EDA or EDAnnexin-coated plates. Importantly, this response was not triggered by soluble EDAnnexin, suggesting a requirement of CAR capping on the CAR-T cell surface (figure 2E). Subsequent experiments using tumor cells as stimuli revealed that EDA CAR-T cells, but not PSMA CAR-T cells, produced IFN- $\gamma$  in response to LLCOVA, FC1242, or F9 tumor cells previously incubated with EDAnnexin protein (figure 2F), highlighting the role of fusion protein as a connector between PS-expressing tumor cells and EDA CAR-T cells. IL-2, TNF- $\alpha$ , IFN- $\gamma$  production and CD69 expression by CD4 and CD8 EDA CAR-T cells in the presence of EDAnnexin and FC1242 tumor cells was also evidenced using flow cytometry (figure 2G,H). Similarly, tumor cells co-incubated with EDAnnexin activated the expression of granzyme B on CD4 and CD8 EDA CAR-T cells (figure 2G,H, respectively) as well as the lytic activity (relative lysis: increment of tumor cell lysis after adding EDAnnexin protein to the culture (figure 2I). However, the lytic activity induced in the presence of the adaptor protein (redirected lysis) appeared somewhat lower compared with that induced when EDA CAR-T cells recognize PM299L cells expressing EDA on their membrane (direct lysis). In fact, while EDA

CAR-T cells lyse PM299L cells expressing high or low levels of EDA in approximately 6 and 15 hours, respectively, the redirected lysis of EDA CAR-T cells towards FC1242 cells in the presence of the EDAnnexin adaptor takes about 30 hours (online supplemental figure 2A). On analyzing immune synapse (IS) formation through confocal microscopy, we noted that the distance between the Golgi apparatus and the IS was much shorter when EDA CAR-T cells targeted EDA in PM299L-EDA cells (direct lysis) as compared with that observed when EDA CAR-T engages the tumor cell (EDA negative) via the adaptor protein EDAnnexin (redirected lysis) (figure 2J and online supplemental figure 2B). In agreement, the F-actin polarization to the IS was also higher in the case of the direct lysis compared with the contact induced by the adaptor molecule EDAnnexin (figure 2K).

Once we confirmed the ability of the EDAnnexin protein to redirect EDA CAR-T cells towards PS-expressing tumors, we proceeded to assess the potential synergistic effect of co-administering EDA CAR-T cells and EDAnnexin protein in vivo using the F9 teratocarcinoma tumor model. First, we studied the biodistribution of <sup>99m</sup>Tc labeled EDAnnexin following intravenous injection in mice bearing F9 tumors. A control protein, EDA-OVA, with a similar molecular weight, was included for comparison. 22 hours post-injection, EDAnnexin was detected in the liver and bone marrow, while EDA-OVA primarily accumulated in kidneys and bladder (figure 3A). Notably, both proteins were detected in the tumor shortly after administration (6 hours), but EDAnnexin persisted in the tumor even after 22 hours (red arrows in figure 3B).

Following the successful tumor-targeting capacity of EDAnnexin in vivo, we investigated the therapeutic efficacy of a combined approach involving the administration of EDA CAR-T cells along with EDAnnexin protein. Previous studies demonstrated that EDA CAR-T cells delay tumor growth in F9 tumor-bearing mice, although complete eradication was not achieved. Subsequently, F9 tumor-bearing mice received a combination treatment of CD4 and CD8 EDA CAR-T cells, followed by administration of EDAnnexin protein for four doses every 48 hours after T-cell transfer (figure 3C). Consistent with previous observations,<sup>11</sup> EDA CAR-T cells effectively delayed tumor growth. While the combined therapy of EDA CAR-T cells and EDAnnexin protein exhibited a modest enhancement in the antitumor response, these improvements did not reach statistical significance (figure 3C).

To validate the use of annexin V-based fusion proteins as adaptor proteins to redirect the lytic activity of CAR-T cells, we generated the BCMAnnexin protein, which combines annexin V with the BCMA antigen, a target used in BCMA CAR-T cell therapy for multiple myeloma. We previously prepared and validated the functionality of a murine anti-BCMA CAR (Navarro *et al*, submitted). BCMAnnexin was produced in *E. coli* and purified using affinity chromatography (figure 3D). BCMAnnexin was able to bind to the surface of FC1242 and PM299L tumor cells similarly to EDAnnexin (figure 3E) and to activate

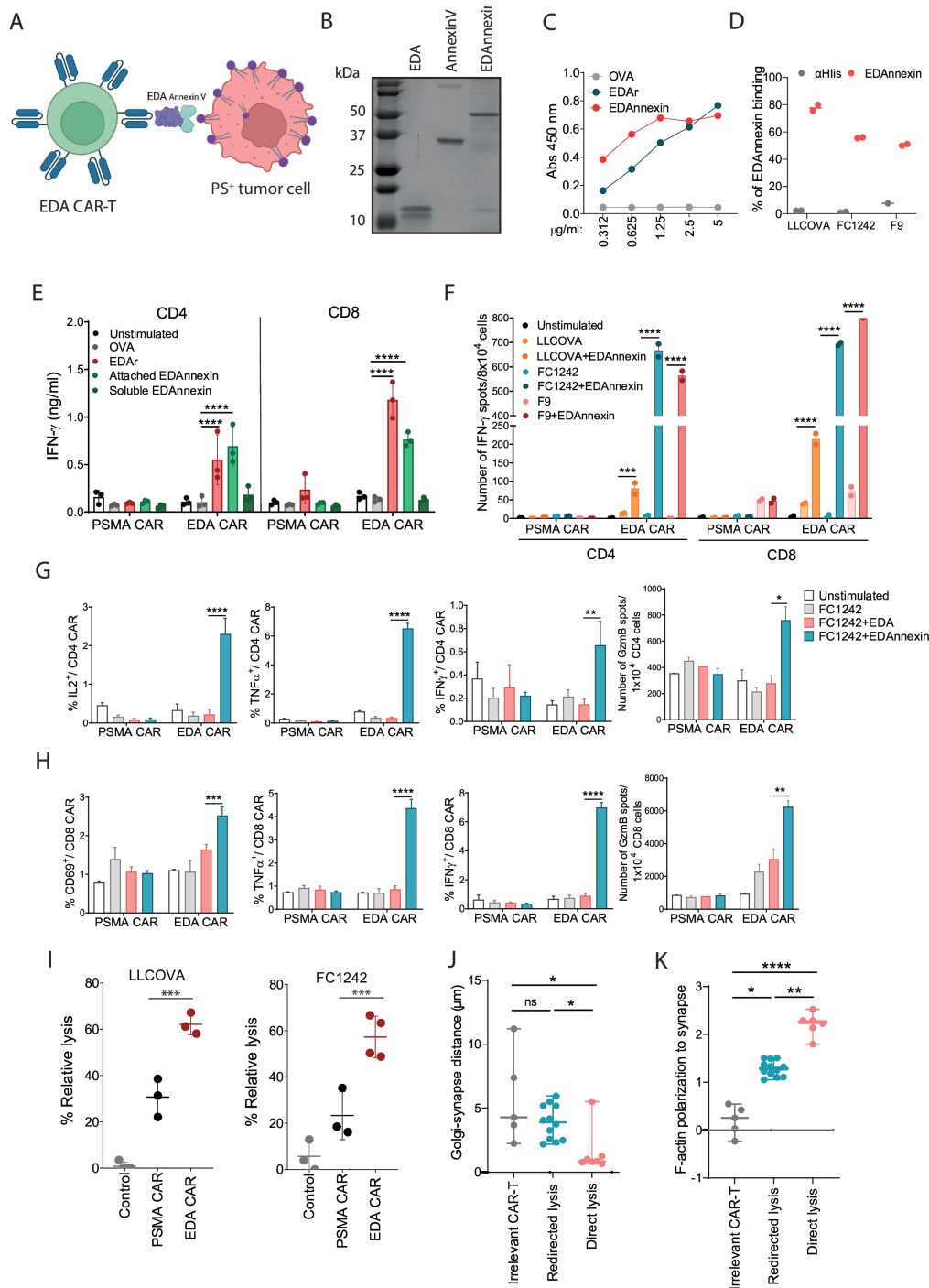


**Figure 2** Annexin V-based adaptor protein to redirect CAR-T cell activity. (A) Scheme representing the strategy to redirect EDA CAR-T cells to PS<sup>+</sup> expressing tumors by using the EDAnnexin adaptor protein. (B) Coomassie blue staining of the recombinant proteins EDA, annexin V and EDAnnexin. (C) EDA recognition by anti-EDA single-chain variable fragment of an antibody F8 measured by ELISA. (D) Binding of EDAnnexin to the PS<sup>+</sup> LLCOVA, FC1242 and F9 tumor cell lines, measured by flow cytometry using anti-His-APC labeled antibodies. (E) IFN- $\gamma$  production by CD4<sup>+</sup> and CD8<sup>+</sup> PSMA CAR-T or EDA CAR-T cells in response to OVA, EDA and EDAnnexin proteins or (F) in response to tumor cell lines in the presence/absence of EDAnnexin. (G) Flow cytometric analysis of CD4<sup>+</sup> (G) and CD8<sup>+</sup> (H) PSMA CAR-T and EDA CAR-T cells after in vitro stimulation with FC1242 tumor cell lines in the presence of EDA or EDAnnexin protein. (I) Relative lytic capacity of PSMA CAR-T or EDA CAR-T cells incubated with LLCOVA or FC1242 tumor cell lines. (J, K) Distance of the Golgi apparatus (J) and measurement of F-actin polarization (K) to the immune synapse when EDA CAR-T cells recognize EDA in the membrane of PM299L-EDA cells (direct lysis) or when EDA CAR-T cells recognize PM299L (EDA negative) through the adaptor protein EDAnnexin (redirected lysis). Data are representative of two to three independently repeated experiments. \* $p < 0.05$ , \*\* $p < 0.01$ , \*\*\* $p < 0.005$ , \*\*\*\* $p < 0.001$ . One-way analysis of variance with Bonferroni multiple comparisons test (E–J). Bars representing the mean and SD are plotted. CAR, chimeric antigen receptor; EDA, extra domain A of fibronectin; IFN, interferon; IL, interleukin; PS, phosphatidylserine; PSMA: Prostate-Specific Membrane Antigen; TNF: Tumor necrosis factor.

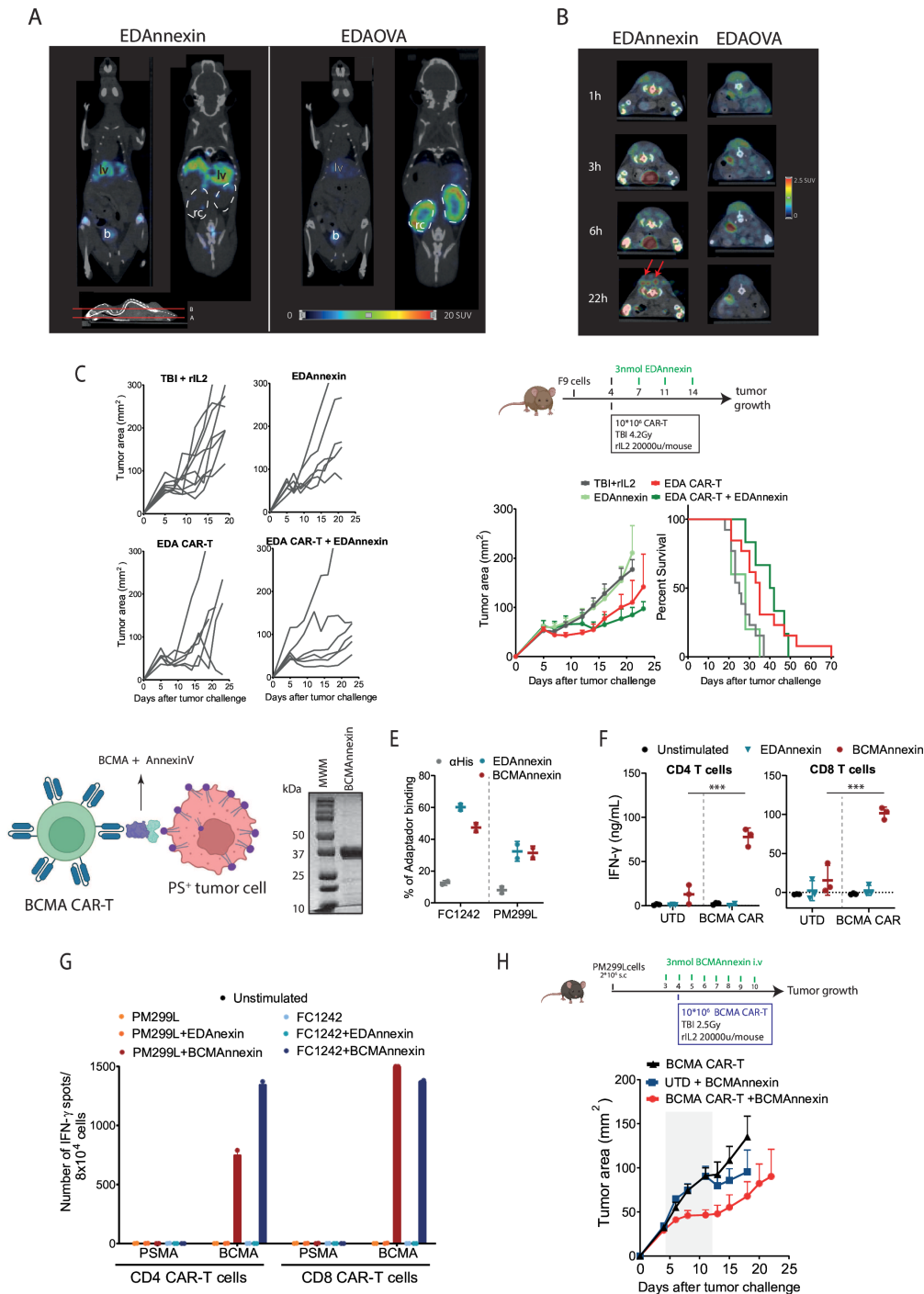


**Figure 3** In vivo antitumor activity of CAR-T cells redirected with annexin V-based fusion proteins protein. (A) In vivo biodistribution of  $^{99m}\text{Tc}$ -labeled EDA-OVA and EDAnnexin proteins in mice bearing F9 tumors, 22 hours after protein injection (B) Biodistribution of the labeled proteins at different time points into the subcutaneous tumor-bearing mice ( $n=3$  mice per group). A representative example is shown). Red arrows highlight the tumor retention of EDAnnexin into the tumor 22 hours after injection. (C) Effect of different CAR-T treatments on tumor progression in mice bearing s.c. F9 tumors ( $n=6-10$  randomized mice per group). Follow-up of the individual tumor areas for each mouse in the different groups. Mean tumor area and mice survival are plotted. (D) Graphical representation of the BCMA CAR-T cell redirection by using BCMAAnnexin adaptor protein through PS<sup>+</sup>tumor cells and Coomassie blue staining of the purified BCMAAnnexin protein. (E) Binding of BCMAAnnexin or EDAnnexin to tumor cells. (F) IFN- $\gamma$  production of BCMA CAR-T cells in response to stimulation with the indicated proteins coated to the culture plates or (G) in response to tumor cells previously incubated with EDAnnexin or BCMAAnnexin proteins. (H) Antitumor effect of BCMA CAR-T cells combined with BCMAAnnexin protein administration in mice bearing PM299L tumors ( $n=6-7$  mice per group). Data are representative of two independent experiments. Two-way analysis of variance and Bonferroni as a post hoc test (F, G). \*\*\* $p < 0.005$ . B, bladder; BCMA, B cell maturation antigen; CAR, chimeric antigen receptor; EDA, extra domain A of fibronectin; IFN, interferon; lv, liver; PS, phosphatidylserine; PSMA: Prostate-Specific Membrane Antigen; rc, renal cortex; rIL, recombinant interleukin; TBI, total body irradiation.

IFN- $\gamma$  production by BCMA CAR-T cells incubated on BCMAnnexin-coated plates (figure 3F). Notably, BCMA CAR-T cells recognized FC1242 and PM299L cells only when these were pre-incubated with the BCMAnnexin adaptor (figure 3G). Importantly, the combination of BCMA CAR-T and BCMAnnexin showed antitumor efficacy in a hepatocarcinoma model based on PM299L cell injection. When C57BL/6 mice bearing PM299L tumors were treated with BCMA CAR-T cells combined with daily doses of 3 mM BCMAnnexin for seven consecutive days, tumor growth was controlled during the administration of the adaptor protein (figure 3H).

### Annexin V CAR-T cells exert a fratricide effect that impairs CAR-T cell production

As an alternative to using an adaptor protein for redirecting CAR-T cell cytotoxicity, we engineered a CAR specific to PS-expressing tumor cells by incorporating annexin V as the CAR ectodomain (Anxa CAR). This construct involved replacing the standard scFv in conventional CARs with the annexin V sequence. A retroviral vector encoding the annexin V CAR fused with eGFP-F2A was designed to facilitate concurrent expression of eGFP and the CAR. Additionally, the control pRubiG plasmid encoding an anti-PSMA CAR was used for comparison (figure 4A). CD4<sup>+</sup> and CD8<sup>+</sup> T cells from C57BL/6 mice transduced with these retroviruses allowed the expression of equivalent levels of GFP for both constructs (figure 4B). While Anxa CAR expression was confirmed using an anti-annexin V antibody (figure 4C), there was an observed decline in cell viability during in vitro expansion, leading to diminished production and lower fold expansion of Anxa CAR-T cells in comparison to PSMA CAR-T cells (figure 4D,E). It has been described that primary human CD8<sup>+</sup> cytotoxic T lymphocytes display exposed PS after T-cell receptor (TCR) stimulation, although this activation-induced PS exposure is less pronounced, reversible and localized within membrane lipid raft domains at the IS.<sup>20</sup> We confirmed the increase of PS exposure on CD4 and CD8 T cells after activation with CD3/CD28 beads used during CAR-T cell production. Thus, although resting CD4 and CD8 T cells exposed low levels of PS in the outer cell membrane, T-cell activation led to an increase in annexin V staining (from 81.7 to 698 MFI in CD4<sup>+</sup> T cells and from 204 to 612 MFI in CD8<sup>+</sup> T cells, figure 4F). Notably, PS upregulation after T-cell activation was clearly below the levels of expression observed in most of the tumor cell lines plotted in figure 1A. Evaluation of the functionality of Anxa CAR-T cells against LLCOVA tumor cells expressing PS revealed a basal IFN- $\gamma$  production activity even in the absence of stimulation with exogenously added PS<sup>+</sup> tumor cells (figure 4G), suggesting a potential fratricidal effect among Anxa CAR-T cells. This fratricide effect is also evidenced when EDA CAR-T are cultured with EDAnnexin. In fact, although the addition of protein EDA-OVA or EDAnnexin does not affect PSMA CAR-T cell production, EDAnnexin significantly reduces EDA CAR-T cell expansion and increases the percentage

of apoptotic cells (Zombie NIR<sup>+</sup>PS<sup>+</sup>) (online supplemental figure 3).

Despite this basal activation of Anxa CAR-T cells, we performed a co-culture experiment with LLCOVA cells, which exhibit high levels of PS. The exposure of PS antigen in LLCOVA cells was enhanced following a 6-hour pre-treatment with the chemotherapeutic agent cisplatin (figure 4H). Co-culturing these cells with CD4<sup>+</sup> and CD8<sup>+</sup> Anxa CAR-T lymphocytes resulted in an increase in IFN- $\gamma$  production compared with their basal activation level (figure 4I). These results might suggest that Anxa CAR-T cells could serve as a promising anti-tumor strategy, provided that the fratricidal effect can be effectively managed or mitigated.

### Low expression of Anxa CAR reduces fratricide effect in vitro and exerts antitumor activity in vivo

We then studied whether reducing the expression level of the CAR on the T-cell membrane could mitigate Anxa CAR-T fratricide. Using flow cytometry, we sorted CAR-T cell products into two groups based on CAR expression levels: CAR<sup>High</sup> and CAR<sup>Low</sup> (figure 5A,B). The cell viability of Anxa CAR<sup>Low</sup>-T was notably enhanced compared with Anxa CAR<sup>High</sup>-T, as evidenced by the percentage of Zombie NIR<sup>+</sup> PS<sup>+</sup> cells (figure 5C). Using videomicroscopy, we could observe a reduction in the number of apoptotic cells and a lower degranulation process in the Anxa CAR<sup>Low</sup>-T as compared with that found in Anxa CAR<sup>High</sup>-T cell cultures (figure 5D,E and online supplemental figure 2C). These data suggest that the fratricidal effect was significantly reduced.

Phenotypic analysis of these two subpopulations showed a less differentiated profile (CD44<sup>+</sup>CD62L<sup>-</sup>) for Anxa CAR<sup>Low</sup>-T cells (figure 5F), lower percentages of CD137<sup>+</sup>PD-1<sup>+</sup> cells (figure 5G) and less exhausted phenotype, characterized by the expression of TIM3 and LAG3 (Lymphocyte Activation Gene-3) (figure 5H), along with a higher number of IFN- $\gamma$  producing cells in response to PS<sup>+</sup> tumor cells (figure 5I).

These findings suggested that lower expression of Anxa CAR may enhance CAR production in T lymphocytes. Normally, T lymphocytes are activated and infected twice with the retroviral vector on day 2 and day 3 of activation. By modifying this protocol eliminating the second infection, a decrease in CAR expression similar to that observed in Anxa CAR<sup>Low</sup>-T levels in figure 5 was achieved. This decrease in Anxa CAR levels (figure 6A) correlated with improved viability of the CAR-T product, as evidenced by a higher percentage of viable cells (figure 6B) and a differentiation phenotype similar to PSMA CAR-T controls (figure 6C).

We did not observe clear differences in senescence markers between Anxa CAR<sup>Low</sup>-T cells and Anxa CAR<sup>High</sup>-T cells. Although there was an increase in HGBM1 levels and a slight decrease in p21 (both associated with senescence) in Anxa CAR<sup>Low</sup>-T cells, IL-6 levels appear to decrease in Anxa CAR<sup>High</sup>-T cells, whereas an increase would be expected in senescent cells. We did not detect

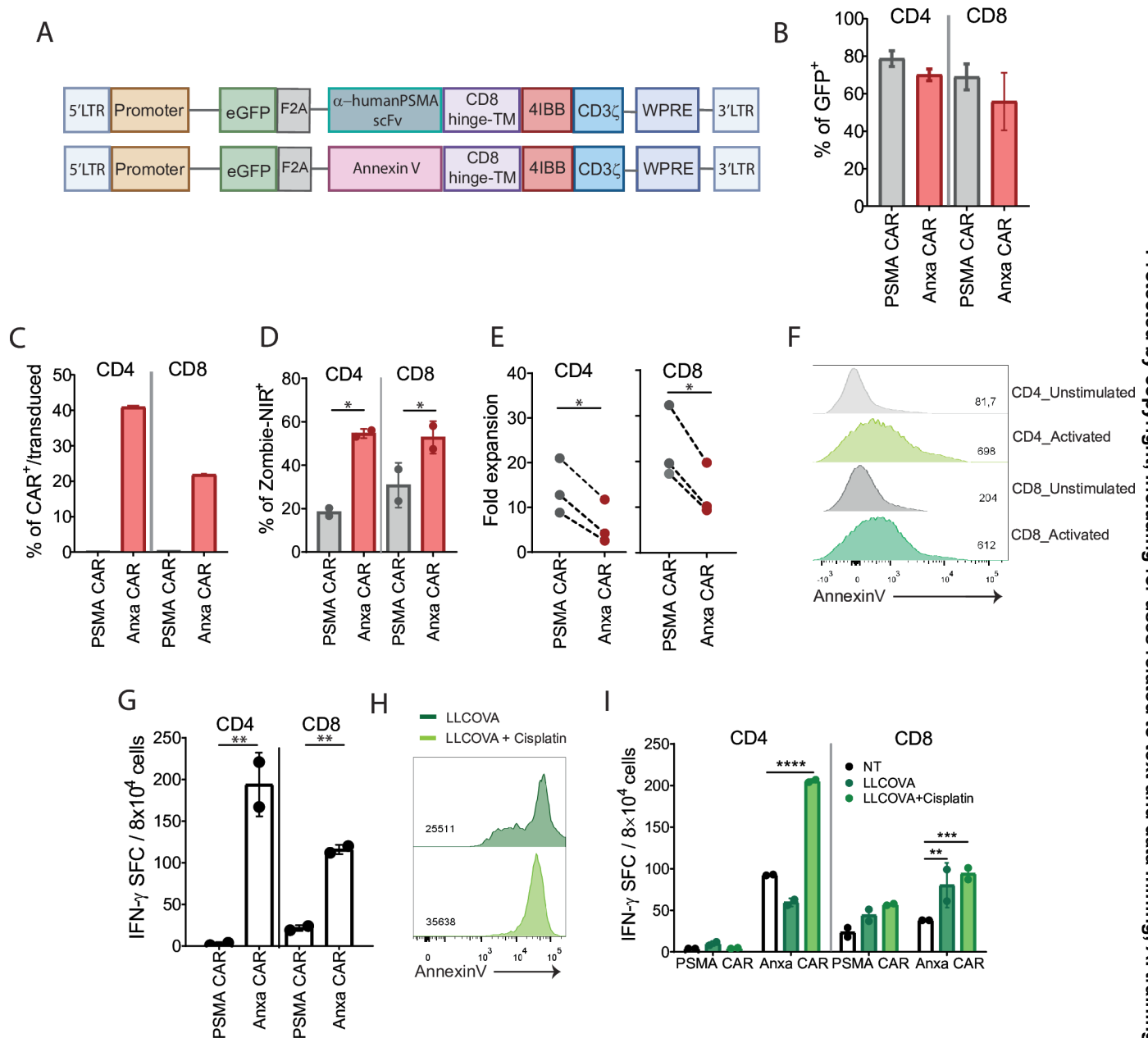


**Figure 4** Anxa CAR-T exerts a fratricide effect that impairs CAR-T cell production. (A) Schematic representation of PSMA and annexin V-based CAR-T cell constructs. (B) CAR expression measured by GFP expression or (C) by staining with anti-annexin V antibody in both CD4<sup>+</sup> and CD8<sup>+</sup> T cells. (D) Cell viability of CD4<sup>+</sup> and CD8<sup>+</sup> PSMA CAR-T and Anxa CAR-T cells measured by flow cytometry as percentage of Zombie NIR<sup>+</sup> cells. (E) Fold expansion capacity of PSMA CAR-T and Anxa CAR-T cells after 5 days of culture. (F) PS expression of unstimulated and activated CD4 and CD8 T cells measured by flow cytometry using annexin-APC. (G) Number of IFN- $\gamma$  producing CD4<sup>+</sup> and CD8<sup>+</sup> CAR-T cells after 5 days of in vitro expansion. (H) PS exposure in LLCOVA tumor cells untreated or treated with cisplatin for 16 hours. (I) Number of IFN- $\gamma$  producing CD4<sup>+</sup> and CD8<sup>+</sup> CAR-T cells in the presence of LLCOVA cells previously treated or not with cisplatin. Data are representative of two to three independently repeated experiments. ns, no significant, \* $p < 0.05$ , \*\* $p < 0.01$ , \*\*\* $p < 0.005$ , \*\*\*\* $p < 0.001$ . Student's t-test (E). One-way ANOVA (D, G) and two-way ANOVA (I) with Bonferroni multiple comparisons test. Bars representing the mean and SD are plotted. ANOVA, analysis of variance; APC: Antigen presenting cell; CAR, chimeric antigen receptor; GFP: Green fluorescence protein; IFN, interferon; PS, phosphatidylserine; PSMA: Prostate-Specific Membrane Antigen.

significant differences in laminin B levels, and MMP2 levels were undetectable (online supplemental figure 4). However, reduced Anxa CAR expression showed a trend towards decreasing the percentage of PD-1<sup>+</sup>CD137<sup>+</sup> cells, although still evidenced a high expression of CD69 (figure 6D) and a high percentage of TIM3<sup>+</sup>LAG3<sup>+</sup> cells,

indicating basal activation possibly triggered by the recognition of PS in the CAR-T cell membrane (figure 6E).

By implementing this modification in the CAR production process, the generation of Anxa CAR<sup>Low</sup>-T cells was enhanced, enabling the assessment of their antitumor efficacy in a tumor model using PM299L cells. Previously,

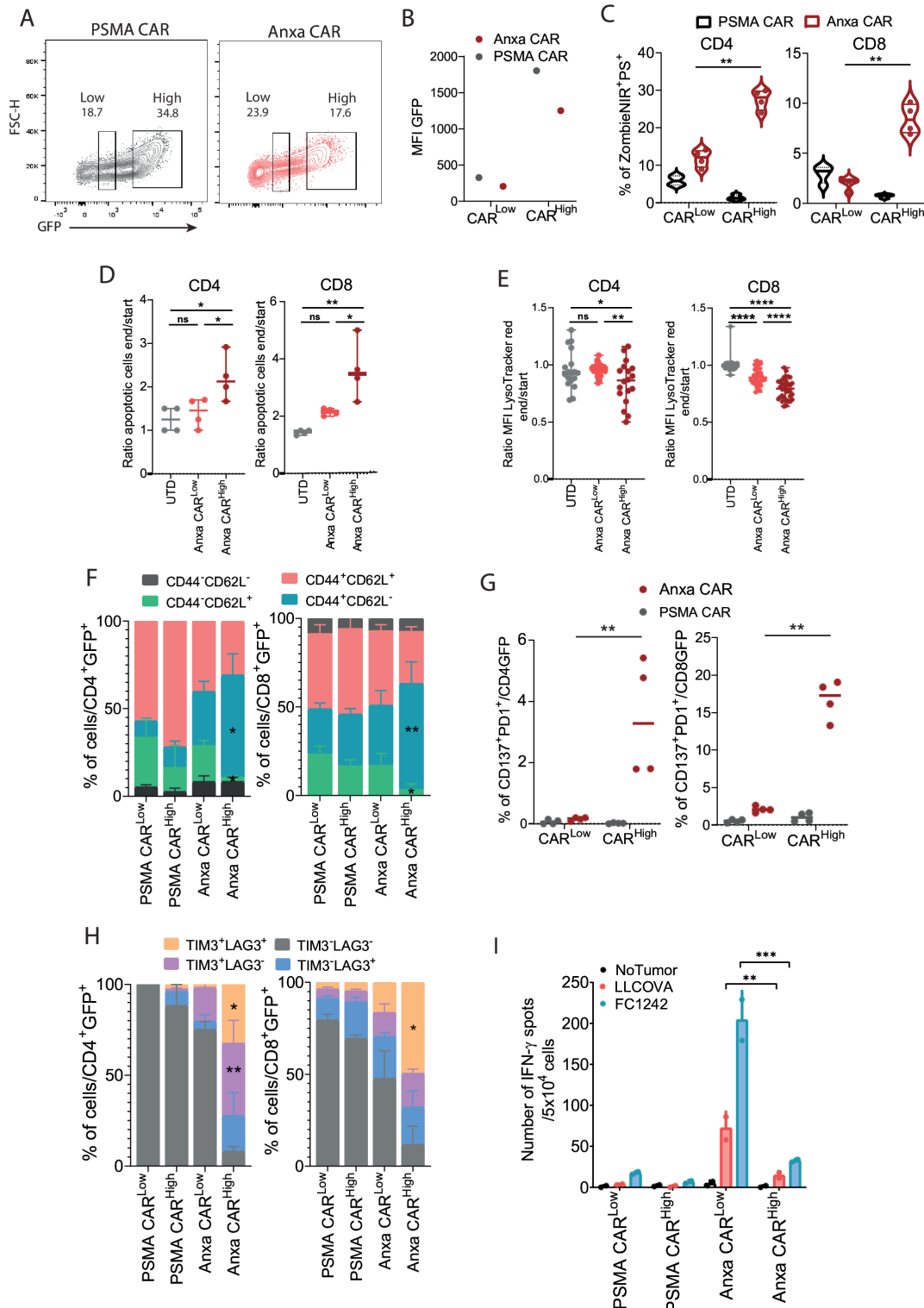


**Figure 5** Anxa CAR<sup>Low</sup>-T had lower fratricide effect in vitro. (A) Level of CAR expression in PSMA CAR-T and Anxa CAR-T cells measured by flow cytometry. (B) Mean fluorescence intensity of GFP present in CAR-T<sup>High</sup> and CAR-T<sup>Low</sup> cells. (C, D, E) Cell viability measured as percentage of ZombieNir<sup>+</sup>PS<sup>+</sup> cells (C), Level of apoptosis (end/start ratio) in cultures of CD4<sup>+</sup> or CD8<sup>+</sup> CAR-T<sup>High</sup> and CAR-T<sup>Low</sup> cells (D), degranulation measured as changes in MFI of LysoTracker staining (end/start ratio) in CD4<sup>+</sup> and CD8<sup>+</sup> CAR-T<sup>High</sup> and CAR-T<sup>Low</sup> cells (E). Phenotype (F), percentage of CD137<sup>+</sup> PD1<sup>+</sup> cells (G) and percentage TIM3<sup>+</sup> and LAG3<sup>+</sup> cells (H) in CAR-T<sup>High</sup> and CAR-T<sup>Low</sup> cells. (I) Number of IFN-γ producing cells in 5x10<sup>4</sup> CAR-T cells after stimulation with LLCOVA or FC1242 tumor cell lines. ns, no significant, \*p<0.05, \*\*p<0.01, \*\*\*p<0.005, \*\*\*\*p<0.001. One-way ANOVA with Bonferroni multiple comparisons test (C, D, E, G) and two-way ANOVA (F, H, I). Data are representative of two independent experiments. Bars representing the mean and SD are plotted. ANOVA, analysis of variance; CAR, chimeric antigen receptor; GFP: green fluorescence protein; IFN, interferon; LAG3: Lymphocyte Activation Gene-3; MFI, mean fluorescence intensity; PS, phosphatidylserine; PSMA: Prostate-Specific Membrane Antigen; TIM3, transmembrane immunoglobulin and mucin 3.

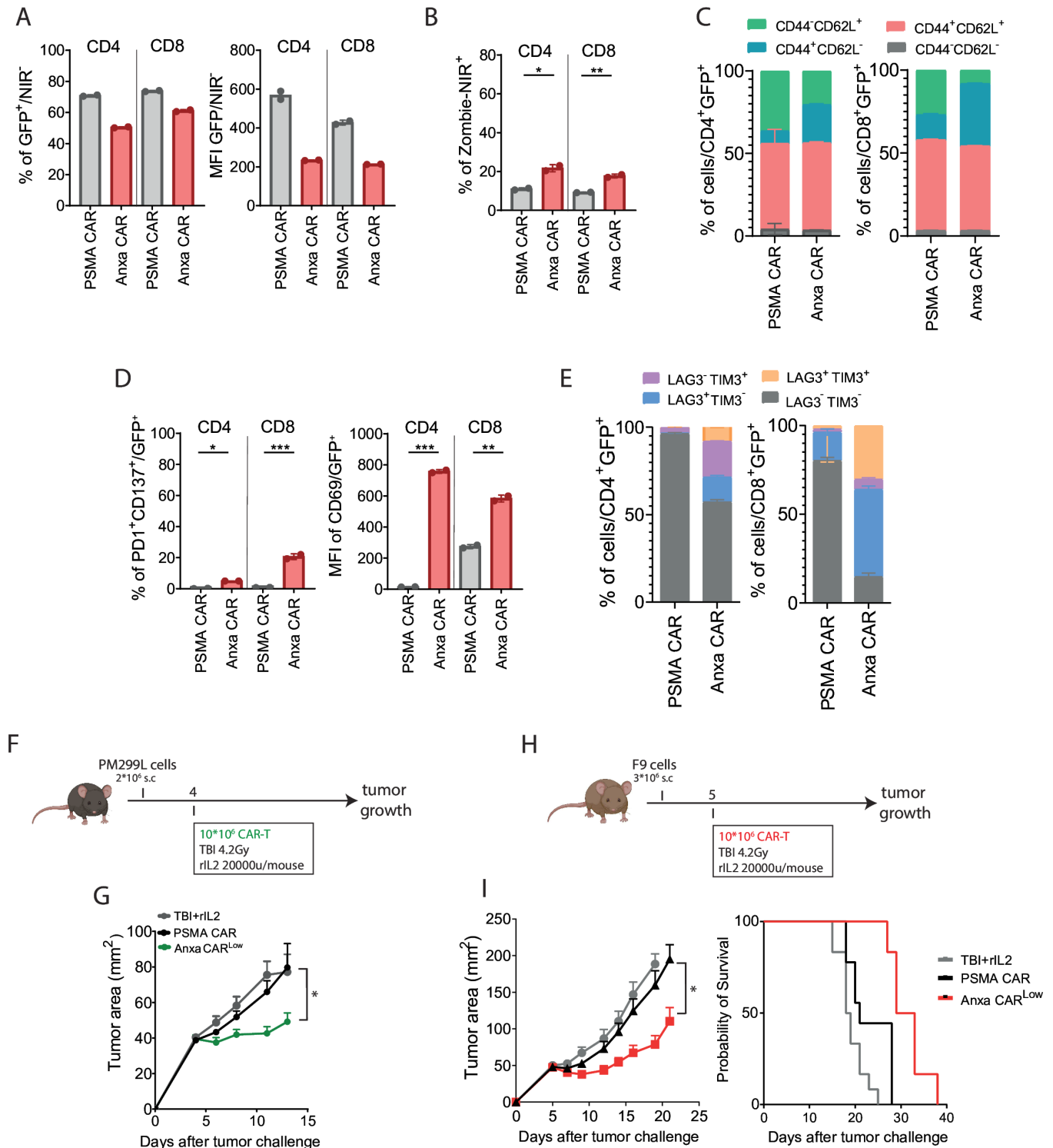


**Figure 6** Anxa CAR<sup>LOW</sup>-T exerts antitumor activity in vivo. (A) CAR-T cell expression and (B) cell viability after one single infection with retrovirus expressing Anxa CAR in CD4<sup>+</sup> and CD8<sup>+</sup> T cells. (C) T-cell phenotype measured by CD44 and CD62L expression, (D) percentage of PD-1<sup>+</sup>CD137<sup>+</sup> cells and CD69<sup>+</sup> cells and (E) percentage of TIM3<sup>+</sup> LAG3<sup>+</sup> cells in PSMA CAR-T and Anxa CAR<sup>LOW</sup>-T cells. (F, H) Graphical scheme of the in vivo experiment in mice bearing PM299L tumors (F) or F9 tumors (H). (G) Tumor progression after treatment of mice with  $5 \times 10^6$  CD4<sup>+</sup> and  $5 \times 10^6$  CD8<sup>+</sup> Anxa CAR<sup>LOW</sup>-T cells or PSMA CAR-T cells (n=10 randomized mice per group). (H) Mean tumor progression and mice survival after treatment of mice with  $5 \times 10^6$  CD4<sup>+</sup> and  $5 \times 10^6$  CD8<sup>+</sup> Anxa CAR<sup>LOW</sup>-T cells or PSMA CAR-T cells in mice bearing F9 tumors (n=6–8 mice per group). (A–E) Data are representative of two independent experiments. Bars representing the mean and SD are plotted. (G, I) Analyzed using one-way-analysis of variance with Bonferroni as a post hoc test. Non-linear fit model (G, I). \*p<0.05, \*\*p<0.01, \*\*\*p<0.005. CAR, chimeric antigen receptor; GFP: Green fluorescence protein; LAG-3: Lymphocyte Activation Gene-3; MFI, mean fluorescence intensity; PD1: Programmed Cell Death Protein 1; rIL, recombinant interleukin; s.c.: subcutaneous route; TBI, total body irradiation; TIM3, transmembrane immunoglobulin and mucin 3.

we demonstrated that Anxa CAR-T cells exhibited the capacity to lyse the PM299L and LLCOVA tumor cell lines, which display higher levels of PS on their surface, whereas they failed to lyse the MM5080 or B16OVA lines, which exhibit lower levels of PS on their surface (online supplemental figure 5). Mice harboring approximately 5 mm diameter PM299L tumors were treated with  $5 \times 10^6$  CD4 and  $5 \times 10^6$  CD8 Anxa CAR<sup>Low</sup>-T cells, PSMA CAR-T cells, or left untreated (figure 6F). Monitoring of tumor progression revealed that treatment with Anxa CAR<sup>Low</sup>-T cells significantly delayed tumor growth when compared with the control groups (figure 6G). In parallel, CAR-T cells labeled with CTV (CellTrace Violet Cell Proliferation Kit, Thermo Fisher) were injected into mice bearing tumors to characterize their proliferative capacity and phenotype. 2 days after injection, Anxa CAR-T cells showed a higher proportion of highly proliferating cells (CTV<sup>Low</sup> cells) in both the spleen and tumor compared with PSMA CAR-T cells. Phenotypic analysis revealed no major differences between the two groups; however, Anxa CAR-T cells seemed to exhibit a slightly more effector-like phenotype (a higher percentage of CD44<sup>+</sup>CD62L<sup>-</sup> cells) and a higher percentage of TIM3<sup>+</sup> and CD69<sup>+</sup> cells, which may indicate a more activated phenotype (online supplemental figure 6). The antitumor effect of Anxa CAR-T cells was also observed in the tumor model based on the administration of the F9 teratocarcinoma cell line (figure 6H,I).

It has been reported that transient exposure of CAR-T cells to the multikinase inhibitor dasatinib can dampen CAR-T signaling and reduce exhaustion, promoting a stem cell memory profile instead of a more exhausted phenotype.<sup>21,22</sup> We tested this strategy to inhibit CAR-T signaling and prevent fratricide during CAR-T manufacturing. Although adding dasatinib during the expansion process reduced the fold expansion of both CD4 and CD8 Anxa CAR-T cells (figure 7A), their phenotypic analysis (in both Anxa CAR<sup>High</sup> and Anxa CAR<sup>Low</sup>-T cells) showed a reduction in CD44<sup>+</sup> CD62L<sup>-</sup> effector T cells and an increase in CD44<sup>+</sup> CD62L<sup>+</sup> cells. Notably, cells incubated with dasatinib exhibited a less exhausted phenotype with a lower number of TIM3<sup>+</sup>LAG3<sup>+</sup> cells in both Anxa CAR<sup>Low</sup> and Anxa CAR<sup>High</sup>-T cell populations (figure 7B,C). We obtained sufficient number of Anxa CAR-T lymphocytes and conducted an antitumor efficacy experiment in a hepatocarcinoma model using PM299L cell injections. In this experiment, we observed a greater antitumor effect in Anxa CAR-T cells that had been treated with dasatinib (figure 7D).

We assessed on-target/off-tumor toxicities in healthy mice after administering  $10 \times 10^6$  Anxa CAR-T cells, comparing groups with and without prior 4Gy TBI. Over 50 days, we monitored mouse weights and serum biochemical parameters on days 0, 5, 10, and 40 post-administration. There were no significant weight changes or alterations in serum levels of ALP, ALT, AST, CRP, AMLY2, or CKMB between the groups. In parallel, a group of mice were sacrificed 10 days after Anxa CAR-T

administration for tissue histological examination (thymus, spleen, lymph nodes, bone marrow, lung, liver), which also showed no significant abnormalities (online supplemental figure 7A–C). We investigated the biodistribution of Anxa CAR-T cells (GFP<sup>ve</sup>) in various tissues and found them in the bone marrow, liver, lungs and the spleen (online supplemental figures 7D and 8A). There were no significant changes in the numbers of CD45 cells, B lymphocytes, T lymphocytes, CD11c<sup>+</sup>, CD11b<sup>+</sup> or NK1.1<sup>+</sup> cells in the bone marrow, liver, lung, lymph nodes, spleen and thymus across different groups, aside from those attributable to 4Gy irradiation (online supplemental figure 8B). Similarly, we did not observe any differences in the percentage of CD45<sup>+</sup> Lineage<sup>-</sup> Sca1<sup>+</sup> progenitor cells in the thymus of mice treated with Anxa CAR-T cells (online supplemental figure 8C). These findings suggest no uncontrolled activation of Anxa CAR-T cells in healthy animals.

Activated T cells can expose some levels of PS on their surface. It could be postulated that Anxa CAR-T injection could compromise the T-cell immune response against other antigens. We evaluated whether a lymphocyte activated by a viral infection could become a target for Anxa CAR-T cells. C57BL/6 mice, infected with recombinant adenoviruses expressing luciferase, received  $15 \times 10^6$  Anxa CAR-T cells or activated T lymphocytes as controls. The decay in luciferase signal assesses the antiviral response. Results showed similar kinetics of infected cell elimination in both the Anxa CAR-T injected mice and control groups. Subsequent analysis of the antiviral response through splenocyte proliferation and IFN- $\gamma$  production revealed no differences between the groups (online supplemental figure 9). The findings suggest that activated lymphocytes do not become targets for Anxa CAR-T cells' lytic action in vivo.

One major concern with using PS as a target for CAR-T cell therapies is the potential for on-target, off-tumor toxicity. To investigate the toxicity of Anxa CAR-T cells under pathological conditions, we conducted an experiment using a DSS (Dextran Sodium Sulfate)-induced colitis model, known for significant inflammation and apoptosis in the colon epithelium.<sup>23</sup> Mice were given DSS in their drinking water for 6 days. Subsequently, one group received a dose of  $15 \times 10^6$  Anxa CAR-T cells, while the other group received untransduced T cells. Both groups experienced rapid weight loss during the initial days of DSS administration. In the experiment, two out of five mice in the control group were euthanized after losing more than 20% of their weight, compared with three out of five mice in the Anxa CAR-T treated group, with no significant difference between the groups (online supplemental figure 10). The surviving mice were able to regain their weight, with no further notable differences observed between the groups.

## DISCUSSION

PS typically localized on the intracellular side of cell membranes, can be externalized to the outer membrane

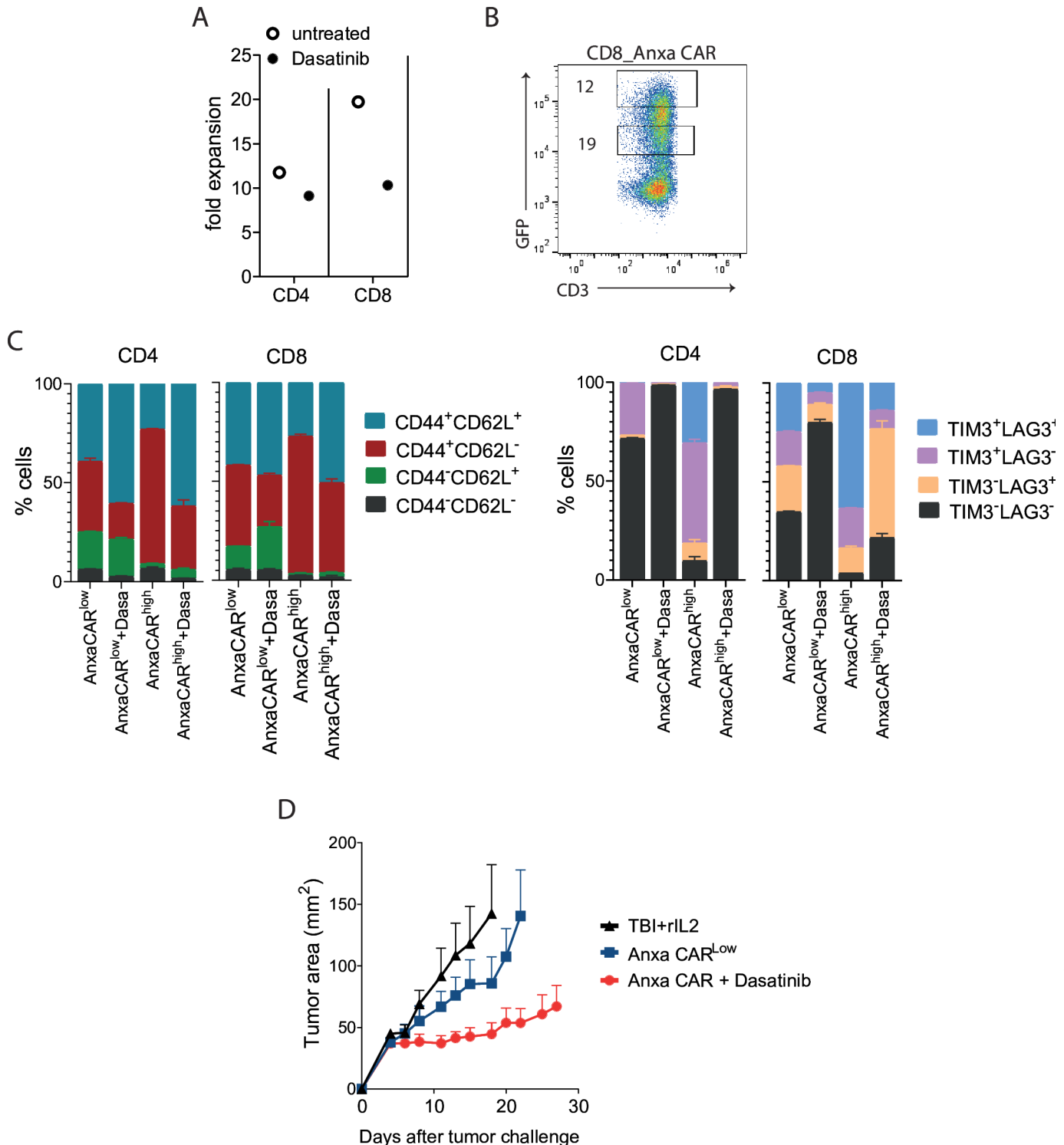


**Figure 7** Effect of transient exposure of CAR-T cells to dasatinib on CAR-T cell expansion, phenotype and antitumor activity. CAR-T cells were expanded in the presence of dasatinib during the manufacturing process. Fold expansion in the presence or absence of dasatinib (A), the level of Anxa CAR expression (B) and phenotypic analysis measured by flow cytometry (C) are plotted. (D) Antitumor effect of Anxa CAR-T cells in mice bearing PM299L tumors (n=6–8 mice per group). CAR, chimeric antigen receptor; GFP: Green fluorescence protein; LAG-3: Lymphocyte Activation Gene-3; rIL, recombinant interleukin; TBI, total body irradiation; TIM3, transmembrane immunoglobulin and mucin 3.

in numerous tumor types due to various environmental factors within the tumor microenvironment. These factors include nutrient deprivation, oxidative stress, hypoxia, and the presence of an immature tumor vasculature.<sup>8</sup>

Confirming previous reports,<sup>24</sup> we have evidenced the PS exposure on the outer leaflet of the cell membrane in several tumor cell lines and tumor tissues from mice inoculated with these cells. Contrary to control splenocytes

lacking PS expression, we observed robust annexin V staining in multiple tumor cell lines, although with varied intensity among cells within the same line. This diversity may be associated with oxidative stress levels at different phases of the cell cycle.<sup>25</sup> The direct correlation observed between the proliferation rate and the level of PS exposure on the membrane suggests that the stress associated with cell proliferation promotes PS exposure. It would be reasonable to speculate that PS exposure in tumor tissue is a dynamic process, influenced by the proliferative status of the cells or the cellular stress they are experiencing at any given moment. Noteworthy, total body irradiation or cisplatin treatment augmented PS exposure, likely due to radiation<sup>26</sup> or chemotherapy-induced oxidative stress mechanisms.<sup>27</sup> These findings indicate the potential of targeting PS for the advancement of CAR-T therapies. In a preliminary investigation, we explored the utility of the bifunctional protein EDAnnexin to redirect the lytic function of EDA CAR-T cells that have demonstrated antitumor efficacy in various tumor models expressing EDA in the tumor ECM and endothelium.<sup>11</sup> This strategy could provide a molecular safety switch to precisely control the adaptor CAR-T cell activity in case of toxicity.<sup>28</sup> In vitro results indicate that this strategy is capable of redirecting the specificity of EDA CAR-T and eliminating PS<sup>+</sup> tumor cells. In vivo biodistribution studies using SPECT imaging in mice injected intravenously with <sup>99m</sup>Tc-labeled EDAnnexin revealed significant accumulation of the protein in the tumor after 22 hours. This distribution profile markedly differed from that of the control protein EDA-OVA, which predominantly localized in the kidneys and bladder. Adaptor molecules smaller than 60 kDa, such as peptides, nanobodies, and scFvs, are typically rapidly cleared via the kidneys and exhibit serum half-lives ranging from 20 to 90 min. Despite the 48 kDa molecular weight of EDAnnexin, it exhibited prolonged retention in the tumor, liver, and bone marrow, possibly due to its binding to PS in apoptotic cells during liver homeostasis and B lymphopoiesis. Subsequent in vivo experiments combining EDA CAR-T with EDAnnexin in the F9 teratocarcinoma model demonstrated a modest enhancement in the antitumor effects of EDA CAR-T when administered with EDAnnexin, although without reaching statistical significance. The discrepancy between the promising in vitro results and the lack of a synergistic effect in vivo suggests the importance of optimizing the administration schedule for the protein. Alternatively, the distribution of the adaptor protein EDAnnexin into the liver or bone marrow may have interfered with the homing of CAR-T cells to the tumor site. In addition to these pharmacokinetic challenges, we observed that the establishment of the immunological synapse between CAR-T and tumor cells aided by the adaptor protein EDAnnexin (indirect lysis) was different from that observed when a direct recognition of the tumor antigen by the CAR is taking place. The distance between the Golgi apparatus and the IS, or the rearrangement of F-actin at the IS, was closer in direct lysis compared with adaptor-mediated lysis. These

factors are crucial for lymphocyte lytic efficacy<sup>29</sup> and may play a significant role in reducing the efficiency of the adaptor-promoted IS. The efficacy of annexin V-based adaptor proteins was confirmed with the BCMAnnexin protein, which successfully redirected the antitumor activity of a BCMA CAR-T against a tumor lacking BCMA expression. These positive results suggest that the steric hindrances will depend on the size of the adaptor or the target antigen in each case.

Annexin V can inhibit prothrombin activation and potentially increase bleeding risk, although this risk is considered low due to the complex nature of coagulation. Clinical studies using isotope-labeled annexin for imaging have not reported significant toxicity,<sup>30</sup> but further evaluation of potential toxicity is necessary. Additional studies are needed to assess the potential for improved efficacy with this adaptor-CAR-T strategy.

Subsequently, we used annexin V to construct a CAR capable of directly targeting PS on tumor cells, eliciting T cell-mediated antitumor responses. The versatility of this Anxa CAR-T lies in its ability to recognize various tumor types expressing PS on their membranes. Anxa CAR-T lymphocytes exhibited potent IFN- $\gamma$  production in response to PS<sup>+</sup> tumor cells. However, the notable expression of PS on activated T lymphocytes led to a fratricidal effect that posed challenges during CAR-T manufacturing. This PS expression on T cells after TCR stimulation had been previously reported as transient, reversible and associated with the IS.<sup>20</sup> Despite the lower levels of PS expression as compared with that observed in tumor cells, it was above the threshold for Anxa CAR-T activation and for triggering fratricide. This phenomenon complicates the in vitro expansion process where cells are frequently in close contact. Our experimentation with retroviral vectors expressing Anxa CAR revealed heterogeneous CAR expression levels on the cell membrane, with cells exhibiting high or low CAR expression. Notably, cells with lower CAR expression displayed a more favorable phenotype characterized by reduced PS expression, improved viability, and lower exhaustion-associated molecules expression. Previous research has highlighted the significant impact of CAR density on CAR-T cell functionality, where elevated CAR levels are linked to heightened tonic signaling and an exhausted cell phenotype marked by increased expression of inhibitory receptors like PD-1 (Programmed Cell Death Protein 1), CTLA-4 (Cytotoxic T-Lymphocyte-Associated Protein 4), LAG3 (Lymphocyte Activation Gene-3), TIM3 (T-cell Immunoglobulin and Mucin-domain containing-3), and TIGIT (T-cell Immunoreceptor with Ig and ITIM domains).<sup>31</sup> A modification to the CAR-T production protocol enabled the generation of Anxa CAR<sup>Low</sup>-T cells, which demonstrated effective antitumor activity in vivo without observable toxicity. These findings suggest that PS can serve as a viable tumor antigen and a promising target for immunotherapies.

Fratricide has been observed in other projects where the target antigen of CAR-T is also expressed in T lymphocytes. Various strategies have been proposed to mitigate

this effect, including silencing the target antigen in T lymphocytes,<sup>32,33</sup> employing protein expression blockers,<sup>34</sup> using high doses of CAR ligand or blocking antibodies to prevent self-recognition and lysis, and incorporating CAR-T signaling inhibitors during manufacturing.<sup>21,22,35</sup> Following this last approach, using dasatinib during Anxa CAR-T cell production enabled us to reduce CAR-T signaling, prevent fratricide, and decrease CAR-T cell exhaustion, thus promoting a stem cell memory profile that resulted in a more effective antitumor response in vivo.

The exposure of PS in tumor tissues is variable, ranging from 20% to 40% of cells. This exposure can potentially be increased through radiotherapy. Administering a local therapeutic radiation dose, typically between 10 and 15 Gy,<sup>36,37</sup> rather than the 4 Gy used in this study for lymphodepletion, may enhance PS exposure and subsequently improve the effectiveness of Anxa CAR-T cell adoptive therapy.

Given the correlation between the proliferative index and PS exposure levels, our results suggest that PS exposure in tumor cells is a dynamic process, influenced by their proliferative status or cellular stress at any tumor site or moment. Despite the limited percentage of PS exposure, it is known that CAR-T cells can affect cells that do not express the target antigen through bystander lytic activity.<sup>38</sup> This involves indirect tumor cell destruction via the activation of immune cells like macrophages and NK cells. Moreover, CAR-T cell-induced cytokines such as IFN- $\gamma$  or TNF- $\alpha$  can directly impact tumor cells by inhibiting proliferation, promoting apoptosis, or reducing angiogenesis apoptosis.<sup>39–42</sup> This bystander effect may aid in eliminating heterogeneous cancer cell populations found in solid tumors. Additionally, cell death within the tumor will lead to increased PS exposure on the cell surface, which will be a direct target for Anxa CAR-T cells or CAR-T cells redirected by annexin V-based adaptor molecules, potentially amplifying the antitumor effect of the therapy. We observed that dead tumor cells expose higher levels of PS and promote greater IFN- $\gamma$  production by CAR-T cells redirected to PS using the annexin V-based adaptor protein (online supplemental figure 11). Further experiments are required to go in depth in these processes.

In summary, targeting PS either by using Anxa CAR-T cells or annexin V-based adaptor proteins might be an attractive strategy for the treatment of a variety of tumors expressing PS naturally or following induction with chemotherapy or radiotherapy, as long as the potential fratricidal effect during the manufacturing process can be overcome.

#### Author affiliations

<sup>1</sup>Program of Immunology and Immunotherapy, CIMA Universidad de Navarra, Pamplona, Spain

<sup>2</sup>Department of Immunology, Ophthalmology and ENT, Universidad Complutense de Madrid, Madrid, Spain

<sup>3</sup>Department of Nuclear Medicine, CIMA Universidad de Navarra, Pamplona, Spain

<sup>4</sup>IdiSNA, Pamplona, Spain

<sup>5</sup>Liver Unit, University Clinic of Navarra, Pamplona, Spain

<sup>6</sup>Radiology, University Clinic of Navarra, Pamplona, Spain

<sup>7</sup>Hemato-Oncology Program, CIMA Universidad de Navarra, Pamplona, Spain

<sup>8</sup>Hematology and Cell Therapy Department, University Clinic of Navarra, Pamplona, Spain

<sup>9</sup>CIBERCV, Madrid, Community of Madrid, Spain

X Noa Martin-Cofreces @noabmartin and Juan Jose Lasarte @jose\_lasarte

**Acknowledgements** We thank Elena Ciordia and Eneko Elizalde for the excellent animal care, the Blood Bank of Navarra (Biobanco, IDISNA, Pamplona) and Laura Guembe (Unidad de Morfología, CIMA, IDISNA, Pamplona) for their collaboration.

**Contributors** Conceptualization: JJJ, CM-O, and TL. JJJ is guarantor of the work. Methodology: CM-O, IS-M, NC, FN, MG, CC, PJ-L, ML, FPa, MC, IP, MI, BS, IV, JRR, FPr, SH-S, AG-M, NM-C, JJJ, TL. Investigation: CM-O, IS-M, SH-S, JRR, FPr, AG-M, NM-C, JJJ and TL. Writing—Original Draft: JJJ and TL. Writing—Review and Editing: all authors. Funding Acquisition: JJJ, FPr and TL. Supervision: JJJ and TL.

**Funding** The study was supported by grants from: Ministerio de Ciencia, Innovación y Universidades and FEDER, UE (MICIU/AEI /10.13039/501100011033, PID2021-1282830A-I00, PID2022-1372650B-I00, PID2022-1418950B-I00, PID2019-108989RB-I00, PLEC2021-008094 MCIN/AEI/10.13039/501100011033, AUTOCART, RTC-2017-6585-1); Gobierno de Navarra Industria (0011-1411-2019-000079 and 0011-1411-2019-000072 Proyecto DESCARTHeS; 0011-1411-2022-000053 and 0011-1411-2022-000088 Proyecto SOCRATHeS; 0011-1411-2023-000105 and 0011-1411-2023-000074 Proyecto DIAMANTE); Instituto de Salud Carlos III co-financed by European Regional Development Fund-FEDER “A way to make Europe” Red de Terapias Avanzadas TERAIV (RD21/0017/0009); Gobierno de Navarra (Departamento de Salud (045-2017; HEPATIL) co-financed (50%) with FEDER funds (UE, FEDER 2014-2020 “A way to make Europe”); Centro de Investigación Biomédica en Red de Cáncer CIBERONC (CB16/12/00489) and CIBERCV (CB16/11/00272); Fundación LaCaixa FLC/PR/HR23/52430018, the European Union, (CARAMBA, SC1-PM-08-2017. Contract 754658), the Innovative Medicines Initiative 2 Joint Undertaking under grant agreement number 945393, T2EVOLVE (this Joint Undertaking receives support from the European Union’s Horizon 2020 Research and Innovation Program; the European Federation of Pharmaceutical Industries and Associations (EFPIA) and the European Hematology Association (EHA); the Paula & Rodger Riney Foundation; Cancer Research UK [C355/A26819], FC AECC and AIRC under the Accelerator Award Program and from the Caja Rural de Navarra.

**Competing interests** None declared.

**Patient consent for publication** Not applicable.

**Ethics approval** This study has been approved by the Comité Ético de Investigación (CEI); Universidad de Navarra, protocols 2019.162 and 2022.055. Participants gave informed consent to participate in the study before taking part.

**Provenance and peer review** Not commissioned; externally peer reviewed.

**Data availability statement** Data are available upon reasonable request. All data relevant to the study are included in the article or uploaded as supplementary information. Not Applicable.

**Supplemental material** This content has been supplied by the author(s). It has not been vetted by BMJ Publishing Group Limited (BMJ) and may not have been peer-reviewed. Any opinions or recommendations discussed are solely those of the author(s) and are not endorsed by BMJ. BMJ disclaims all liability and responsibility arising from any reliance placed on the content. Where the content includes any translated material, BMJ does not warrant the accuracy and reliability of the translations (including but not limited to local regulations, clinical guidelines, terminology, drug names and drug dosages), and is not responsible for any error and/or omissions arising from translation and adaptation or otherwise.

**Open access** This is an open access article distributed in accordance with the Creative Commons Attribution Non Commercial (CC BY-NC 4.0) license, which permits others to distribute, remix, adapt, build upon this work non-commercially, and license their derivative works on different terms, provided the original work is properly cited, appropriate credit is given, any changes made indicated, and the use is non-commercial. See <http://creativecommons.org/licenses/by-nc/4.0/>.

#### ORCID iDs

Alvaro Gómez-Morón <http://orcid.org/0000-0003-1918-990X>

Marta Larrayoz <http://orcid.org/0000-0001-6097-8244>

Sandra Hervás-Stubbs <http://orcid.org/0000-0003-3391-1516>

## REFERENCES

- 1 Doran AC, Yurdagül A, Tabas I. Efferocytosis in health and disease. *Nat Rev Immunol* 2020;20:254–67.
- 2 Graham DK, DeRyckere D, Davies KD, et al. The TAM family: phosphatidylinositol sensing receptor tyrosine kinases gone awry in cancer. *Nat Rev Cancer* 2014;14:769–85.
- 3 Zagórska A, Través PG, Lew ED, et al. Diversification of TAM receptor tyrosine kinase function. *Nat Immunol* 2014;15:920–8.
- 4 Taniguchi H, Yamada T, Wang R, et al. AXL confers intrinsic resistance to osimertinib and advances the emergence of tolerant cells. *Nat Commun* 2019;10:259.
- 5 Taylor A, Verhagen J, Blaser K, et al. Mechanisms of immune suppression by interleukin-10 and transforming growth factor-beta: the role of T regulatory cells. *Immunology* 2006;117:433–42.
- 6 Chang W, Fa H, Xiao D, et al. Targeting phosphatidylinositol for Cancer therapy: prospects and challenges. *Theranostics* 2020;10:9214–29.
- 7 Ran S, Thorpe PE. Phosphatidylinositol is a marker of tumor vasculature and a potential target for cancer imaging and therapy. *Int J Radiat Oncol Biol Phys* 2002;54:1479–84.
- 8 Vallabhapurapu SD, Blanco VM, Sulaiman MK, et al. Variation in human cancer cell external phosphatidylinositol is regulated by flippase activity and intracellular calcium. *Oncotarget* 2015;6:34375–88.
- 9 Frey B, Schildkopf P, Rödel F, et al. AnnexinA5 renders dead tumor cells immunogenic--implications for multimodal cancer therapies. *J Immunotoxicol* 2009;6:209–16.
- 10 Birge RB, Boeltz S, Kumar S, et al. Phosphatidylinositol is a global immunosuppressive signal in efferocytosis, infectious disease, and cancer. *Cell Death Differ* 2016;23:962–78.
- 11 Martín-Otal C, Lasarte-Cia A, Serrano D, et al. Targeting the extra domain A of fibronectin for cancer therapy with CAR-T cells. *J Immunother Cancer* 2022;10:e004479.
- 12 Sánchez-Moreno I, Lasarte-Cia A, Martín-Otal C, et al. Tethered IL15-IL15R $\alpha$  augments antitumor activity of CD19 CAR-T cells but displays long-term toxicity in an immunocompetent lymphoma mouse model. *J Immunother Cancer* 2024;12:e008572.
- 13 Rybak JN, Roesli C, Kaspar M, et al. The extra-domain A of fibronectin is a vascular marker of solid tumors and metastases. *Cancer Res* 2007;67:10948–57.
- 14 Lasarte JJ, Casares N, Gorraiz M, et al. The extra domain A from fibronectin targets antigens to TLR4-expressing cells and induces cytotoxic T cell responses in vivo. *J Immunol* 2007;178:748–56.
- 15 Voci S, Pangua C, Martínez-Ohárriz MC, et al. Gliadin nanoparticles for oral administration of bioactives: Ex vivo and in vivo investigations. *Int J Biol Macromol* 2023;249:126111.
- 16 Casares N, Rudilla F, Arribillaga L, et al. A peptide inhibitor of FOXP3 impairs regulatory T cell activity and improves vaccine efficacy in mice. *J Immunol* 2010;185:5150–9.
- 17 Lozano T, Chocarro S, Martín C, et al. Genetic Modification of CD8<sup>+</sup> T Cells to Express EGFR: Potential Application for Adoptive T Cell Therapies. *Front Immunol* 2019;10:2990.
- 18 Martín-Cófreces NB, Rojas-Gomez A, Dosil SG, et al. Rapid Visualization of Intracellular Vesicle Events During Synaptic Stimulation. *Methods Mol Biol* 2021;2346:105–20.
- 19 Calabia-Linares C, Robles-Valero J, de la Fuente H, et al. Endosomal clathrin drives actin accumulation at the immunological synapse. *J Cell Sci* 2011;124:820–30.
- 20 Fischer K, Voelkl S, Berger J, et al. Antigen recognition induces phosphatidylinositol exposure on the cell surface of human CD8<sup>+</sup> T cells. *Blood* 2006;108:4094–101.
- 21 Weber EW, Lynn RC, Sotillo E, et al. Pharmacologic control of CAR-T cell function using dasatinib. *Blood Adv* 2019;3:711–7.
- 22 Weber EW, Parker KR, Sotillo E, et al. Transient rest restores functionality in exhausted CAR-T cells through epigenetic remodeling. *Science* 2021;372:eaba1786.
- 23 Araki Y, Mukaiyoshi K, Sugihara H, et al. Increased apoptosis and decreased proliferation of colonic epithelium in dextran sulfate sodium-induced colitis in mice. *Oncol Rep* 2010;24:869–74.
- 24 Riedl S, Rinner B, Asslaber M, et al. In search of a novel target - phosphatidylinositol exposed by non-apoptotic tumor cells and metastases of malignancies with poor treatment efficacy. *Biochim Biophys Acta* 2011;1808:2638–45.
- 25 Patterson JC, Joughin BA, van de Kooij B, et al. ROS and Oxidative Stress Are Elevated in Mitosis during Asynchronous Cell Cycle Progression and Are Exacerbated by Mitotic Arrest. *Cell Syst* 2019;8:163–7.
- 26 Azzam EI, Jay-Gerin JP, Pain D. Ionizing radiation-induced metabolic oxidative stress and prolonged cell injury. *Cancer Lett* 2012;327:48–60.
- 27 Ramkumar V, Mukherjee D, Dhukhwa A, et al. Oxidative Stress and Inflammation Caused by Cisplatin Ototoxicity. *Antioxidants (Basel)* 2021;10:1919.
- 28 Arndt C, Fasslrunner F, Loureiro LR, et al. Adaptor CAR Platforms-Next Generation of T Cell-Based Cancer Immunotherapy. *Cancers (Basel)* 2020;12:1302.
- 29 Cassioli C, Patrussi L, Valitutti S, et al. Learning from TCR Signaling and Immunological Synapse Assembly to Build New Chimeric Antigen Receptors (CARs). *Int J Mol Sci* 2022;23:14255.
- 30 Belhocine TZ, Blankenberg FG, Kartachova MS, et al. (99m)Tc-Annexin A5 quantification of apoptotic tumor response: a systematic review and meta-analysis of clinical imaging trials. *Eur J Nucl Med Mol Imaging* 2015;42:2083–97.
- 31 Rodríguez-Marquez P, Calleja-Cervantes ME, Serrano G, et al. CAR density influences antitumor efficacy of BCMA CAR T cells and correlates with clinical outcome. *Sci Adv* 2022;8:eabo0514.
- 32 Cooper ML, Choi J, Staser K, et al. An “off-the-shelf” fratricide-resistant CAR-T for the treatment of T cell hematologic malignancies. *Leukemia* 2018;32:1970–83.
- 33 O’Neal J, Ritchey JK, Cooper ML, et al. CS1 CAR-T targeting the distal domain of CS1 (SLAMF7) shows efficacy in high tumor burden myeloma model despite fratricide of CD8<sup>+</sup>CS1 expressing CAR-T cells. *Leukemia* 2022;36:1625–34.
- 34 Png YT, Vinanica N, Kamiya T, et al. Blockade of CD7 expression in T cells for effective chimeric antigen receptor targeting of T-cell malignancies. *Blood Adv* 2017;1:2348–60.
- 35 Breman E, Demoulin B, Agaugué S, et al. Overcoming Target Driven Fratricide for T Cell Therapy. *Front Immunol* 2018;9:2940.
- 36 Gupta A, Probst HC, Vuong V, et al. Radiotherapy promotes tumor-specific effector CD8<sup>+</sup> T cells via dendritic cell activation. *J Immunol* 2012;189:558–66.
- 37 Lai JZ, Zhu YY, Ruan M, et al. Local Irradiation Sensitized Tumors to Adoptive T Cell Therapy via Enhancing the Cross-Priming, Homing, and Cytotoxicity of Antigen-Specific CD8 T Cells. *Front Immunol* 2019;10:2857.
- 38 Kara E, Jackson TL, Jones C, et al. Mathematical modeling insights into improving CAR T cell therapy for solid tumors with bystander effects. *NPJ Syst Biol Appl* 2024;10:105.
- 39 Langaas V, Shahzidi S, Johnsen JI, et al. Interferon-gamma modulates TRAIL-mediated apoptosis in human colon carcinoma cells. *Anticancer Res* 2001;21:3733–8.
- 40 Mazzolini G, Narvaiza I, Martínez-Cruz LA, et al. Pancreatic cancer escape variants that evade immunogene therapy through loss of sensitivity to IFN $\gamma$ -induced apoptosis. *Gene Ther* 2003;10:1067–78.
- 41 Coughlin CM, Salhany KE, Gee MS, et al. Tumor cell responses to IFN $\gamma$  affect tumorigenicity and response to IL-12 therapy and antiangiogenesis. *Immunity* 1998;9:25–34.
- 42 Qin Z, Schwartzkopff J, Pradera F, et al. A critical requirement of interferon gamma-mediated angiostasis for tumor rejection by CD8<sup>+</sup> T cells. *Cancer Res* 2003;63:4095–100.